Linker Chemistry Determines Secondary Structure of p53(14−29) in Peptide Amphiphile Micelles

ARTICLE *in* BIOCONJUGATE CHEMISTRY · FEBRUARY 2010

Impact Factor: 4.51 · DOI: 10.1021/bc900383m · Source: PubMed

6 AUTHORS, INCLUDING:

Dimitris Missirlis
Max Planck Institute for Intelligent System…
14 PUBLICATIONS **512** CITATIONS
SEE PROFILE

Mark Kastantin
University of Colorado Boulder
39 PUBLICATIONS **1,264** CITATIONS
SEE PROFILE

Badriprasad Ananthanarayanan
University of California, Berkeley
16 PUBLICATIONS **193** CITATIONS
SEE PROFILE

Matthew Tirrell
University of Chicago
467 PUBLICATIONS **12,520** CITATIONS
SEE PROFILE

Linker Chemistry Determines Secondary Structure of $p53_{14-29}$ in Peptide Amphiphile Micelles

Dimitris Missirlis,*[,†,‡] Marc Farine,[†] Mark Kastantin,[†] Badriprasad Ananthanarayanan,[†] Thorsten Neumann,[†,‡] and Matthew Tirrell[†,‡]

Department of Chemical Engineering and Materials and Materials Research Laboratory, University of California, Santa Barbara, California 93106, and Department of Bioengineering, University of California, Berkeley, California, 94720. Received September 1, 2009; Revised Manuscript Received February 9, 2010

Biofunctional micelles formed via self-assembly of synthetic peptide-lipid conjugates are a class of promising biomaterials with applications in drug delivery and tissue engineering. The micelle building block, termed peptide amphiphile, consists of a lipid-like chain covalently linked through a spacer to a peptide headgroup. Self-assembly results in formation of a hydrophobic core surrounded by a dense shell with multiple, functional peptides. We report here on the effect that different linkers between a palmitic tail and a bioactive peptide ($p53_{14-29}$) have on headgroup secondary structure. Peptide $p53_{14-29}$ may act as an inhibitor of the interaction between tumor suppressor p53 and human double minute-2 (hDM2) proteins by binding hDM2 in a partially helical form, leading to the release of p53 and the induction of apoptosis in certain tumors. Circular dichroism and fluorescence spectroscopy data revealed that the extent and type of secondary structure of $p53_{14-29}$ are controlled through size and hydrogen bond potential of the linker. In addition, the structure of the self-assembled micelles was influenced through linker-dependent altered headgroup interactions. This study provides insight into the mechanisms through which headgroup structuring occurs on peptide amphiphile micelles, with implications on the bioactivity, stability, and morphology of the self-assembled entities.

INTRODUCTION

Self-assembly of peptide amphiphiles (PAs) represents a versatile methodology for preparation of nanostructures with defined shapes and functionalities (*1, 2*). PAs are composed of a hydrophobic segment, generally a single- or double-alkyl tail, linked to a hydrophilic peptide "headgroup". An appealing way to view the supramolecular aggregates formed by PAs in aqueous solutions is as protein analogous micelles held together by hydrophobic interactions in their interior and presenting a high density of functional peptides on their surface. Through appropriate PA design, self-assembly can lead to formation of fibrous scaffolds similar to extracellular matrix proteins for cell attachment and growth (*3, 4*); with different PA molecular architectures, colloidal structures can be prepared to mimic soluble globular protein function (*5*−*7*).

In order to harness the full potential of PAs as building blocks, appropriate functional peptide presentation is required, which can be achieved via control of monomer interactions. The hydrophobic effect is the predominant driving force responsible for self-assembly; however, in contrast to traditional, low molecular weight detergents, the more complex peptide headgroup may provide additional stabilizing interactions such as reversible disulfide formation (*8, 9*), hydrogen bonding (*10*−*12*), and electrostatic bridging between neighboring peptide chains (*3, 13*). A direct consequence and particularly attractive feature of these interactions in the tethered, close-packed surface of the self-assembled structure is their ability to induce peptide folding in distinct secondary structure motifs, thus displaying peptides in a more native manner (*14*).

Conformational sensitivity is key in achieving specificity in biomolecular interactions. The spatial arrangement of amino acids resulting from folding of the polypeptide chain determines the activity of the protein or enzyme. The same sequence folded in a different manner usually has reduced or even altered activity as is most strikingly evidenced in the activity of misfolded proteins. Thus, the ability to mimic naturally occurring secondary structure motifs and present them on supramolecular constructs could lead to development of more potent peptide ligands/inhibitors. A very common protein-folding pattern is the α helix, which possesses diverse functionalities ranging from protein−protein interactions (*15*) and protein−DNA interactions (*16*) to cell membrane pore formation (*17*). Formation of α-helical domains normally occurs upon protein folding into the native protein conformation. Their typical size is 7−14 residues long corresponding to 2−3 helical turns. However, when the same peptide sequence is isolated from the protein it loses its folding ability. The reasons for this loss of secondary structure are primarily the increase in entropy associated with peptide freedom to probe a larger conformational space and the lack of stabilizing forces from neighboring parts of the protein.

To counterbalance the entropic cost of folding, several approaches have been explored (*18*). Adsorption of the peptide on a surface (*19*) or inside a host template (*20*) have both shown to help in helical stabilization. Chemical modification of the peptide with unnatural amino acids and subsequent cross-linking of the side chains has also proven to provide enough stabilizing energy for helix formation (*21*−*26*). Alternatively, the side chains of appropriately inserted natural amino acids (e.g., histidines) can be used for helix stabilization through metal complexation (*21, 27*). Our group as well as others have shown that secondary structure can be induced in a number of different peptides also as a result of their hydrophobic modification with a lipid tail and subsequent self-assembly into micelles (*6, 14, 28, 29*). Crowding effects and conformational

* Corresponding author. Dimitris Missirlis Materials Research Laboratory, University of California, Santa Barbara, CA 93106, Tel. 805 452 6319, Fax. 805 893 8124, E-mail dimis@engineering.ucsb.edu.
† University of California, Santa Barbara.
‡ University of California, Berkeley.

10.1021/bc900383m
Published on Web 02/18/2010

Scheme 1. Schematic Representation of the Peptide Amphiphiles Used in This Study (A) and Proposed Self-Assembly Scheme (B)

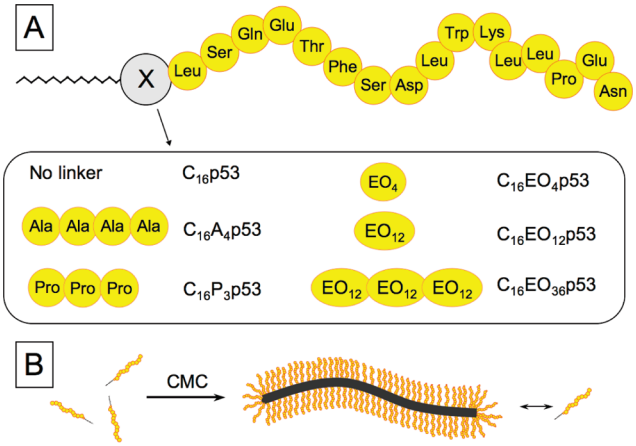

constraints due to dense surface "tethering" of peptide chains on the surface of the micelles are presumed to be the driving forces for assembly (*30, 31*). The type of secondary structure adopted is not solely dictated by the amino acid sequence of the peptide, as has been seen by the folding of the same peptide on a surface into different motifs (*32*). Such observations are reminiscent of peptide misfolding associated with a number of important diseases, e.g., amyloid-β fiber formation (*33*).

Here, we have studied secondary structure conformation of a bioactive peptide in peptide amphiphile micelles and how it is affected by incorporation of different linkers between the peptide and the hydrophobic palmitoyl tail. The peptide we used is derived from the hDM2 binding region of tumor suppressor p53 and has shown potential as an inhibitor of the p53-hDM2 interaction with concomitant reactivation of apoptotic pathways in appropriate cancer cells (*34*). Moreover, peptide activity is linked to its propensity to fold into a short α helix (*23, 35*), and enhanced hDM2 binding of the peptide was reported when helicity was induced through a stapling mechanism (*23*), revealing the importance that secondary structure plays in this protein−protein interaction. Our main goal was to gain understanding of the factors that control peptide folding and supramolecular structure and how these can be manipulated through chemical design of the micelle building block.

EXPERIMENTAL PROCEDURES

Peptide Amphiphile Synthesis. Peptide $p53_{14-29}$ (sequence: LSQETFSDLWKLLPEN) on a Rink amide resin was purchased from Anaspec. Peptide amphiphiles were synthesized from resin-bound peptides using manual Fmoc solid-phase synthesis as previously described (*36*). Following cleavage from the resin, peptide amphiphiles were purified using high-performance liquid chromatography (HPLC; Shimadzu Corporation) on a reverse-phase C_4 column (Vydac), with gradients of acetonitrile in water, containing 0.1% trifluoracetic acid (TFA). A list of the peptide amphiphiles synthesized is presented in Scheme 1 and the chemical structures are shown in Supporting Information Figure S1. Identity of the peptide amphiphiles was verified by electrospray ionization mass spectrometry (Supporting Information Table S1) and purity was determined using analytical HPLC on a reverse-phase C_4 column (Vydac). Peptide amphiphiles with purity greater than 95% were used.

Micelle Preparation. Peptide amphiphiles were dissolved in a 1:1 mixture of chloroform and methanol. The organic solvents were then evaporated under N_2 flow eventually forming a film on a glass vial wall. The film was then dried in vacuum and hydrated in water or buffer at 60 °C for 1 h. Mixed micelles were prepared by hydrating PA films with solutions of Tween 40 (Sigma) at different Tween/PA ratios at 60 °C for 1 h. Following cooling to room temperature, the aqueous micelle solutions were filtered through a 0.45 μm polycarbonate syringe filter (Millipore). All samples were stored at 4 °C and used within 1 week of preparation unless otherwise noted. Fluorescence, circular dichroism, and light scattering measurements were not significantly changed within this time period.

Fluorescence Spectroscopy. Fluorescence was recorded using a Varian Cary Eclipse fluorescence spectrophotometer, equipped with a cuvette holder thermostatted at 25 °C, unless otherwise noted. In steady-state fluorescence emission measurements, tryptophan (Trp) was excited at 280 nm and emission was recorded between 300 and 400 nm. Steady-state anisotropy was measured using manual polarization lenses and calculated using the following equation (*37*):

$$r = \frac{I_{VV} - I_{VH}I_{HV}/I_{HH}}{I_{VV} + 2I_{VH}I_{HV}/I_{HH}} \quad (1)$$

I_{VV}, I_{HH}, I_{VH}, and I_{HV} are fluorescence intensities; the subscripts V and H stand for vertical and horizontal orientations of polarizers, respectively, with the first subscript corresponding to the excitation light and the second to the emitted light. Values of anisotropy presented here are averaged over a range of wavelengths (340−370 nm) after excitation at 290 nm.

Fluorescence quenching measurements were performed after addition of aliquots of a freshly prepared 5 M KI to a solution of p53 or C_{16}p53 (100 uM). Dynamic (collisional) quenching is described by the Stern−Volmer equation (*38*)

$$\frac{I_0}{I} = 1 + K_{SV}[Q] \quad (2)$$

where $[Q]$ is the quencher (KI) concentration, I_0 and I are the fluorescence intensities in the absence and presence of quencher respectively, and K_{SV} is the Stern−Volmer constant. The slope of the plot I_0/I against [KI] gives K_{SV}.

Pyrene Fluorescence Measurements. Dried peptide amphiphile films were dissolved in aqueous pyrene stock solution (6×10^{-7} M) containing traces of tetrahydrofuran (THF) and left to equilibrate at 37 °C for 1 h. Fluorescence emission spectra were recorded at different PA concentrations and the intensity ratio of the third (I_3) to the first (I_1) vibrational band of pyrene was determined. The critical micellar concentration (cmc) was determined as the concentration at the onset of I_3/I_1 ratio increase. The equilibrium constant K_v for partitioning of pyrene between the micellar and aqueous phase was estimated using the equation

$$\frac{F - F_{min}}{F_{max} - F} = \frac{K_v x_{core}(C - \text{cmc})}{\rho_{core}} \quad (3)$$

F_{min}, F_{max}, and F are the minimum, maximum, and intermediate intensity ratio (I_1/I_3), respectively, x_{core} is the micellar core weight fraction and ρ_{core} the density of that core.

Circular Dichroism. CD spectra of PA solutions were acquired using an Olis RSM spectrophotometer in the far UV region (190−250 nm) using quartz cuvettes of 0.5 mm path length. Baseline spectra were subtracted from sample spectra and smoothed using the software supplied by the manufacturer. Mean residual ellipticity, θ, as a function of wavelength, is presented. Temperature scans were performed from 10 to 80 °C to monitor peptide folding stability. It is important to note that using our experimental setup there was a cutoff at approximately 200 nm when PBS 10 mM was used due to buffer component absorption.

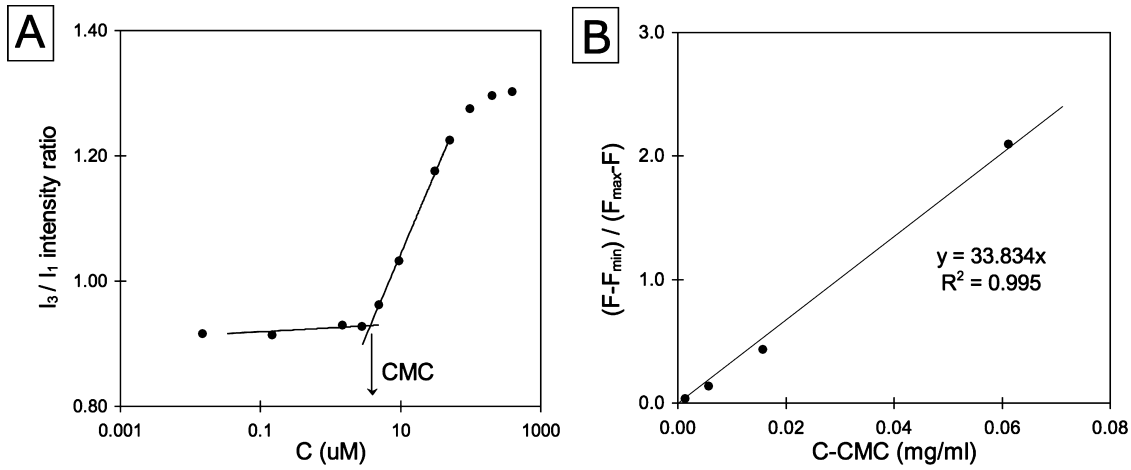

Figure 1. Critical micelle concentration (cmc) determination of C_{16}p53 in PBS 10 mM using the pyrene solubilization method. The onset of increase of the I_3/I_1 intensity ratio of pyrene emission peaks corresponds to the cmc (A). The partition coefficient of pyrene between the hydrophobic core and the aqueous phase is derived from the slope of (B) using eq 3.

Dynamic Light Scattering (DLS). Micelle size was assessed using a DLS system (Brookhaven Instruments) that consisted of an avalanche photodiode detector to measure scattering intensity from a 632.8 nm HeNe laser (Melles Griot) as a function of delay time. Temperature was maintained at 25.0 ± 0.1 °C using a circulating water bath unless otherwise noted. The first-order autocorrelation function was measured at different angles between 40° and 120° to cover a range of scattering wave vector, q, of 0.0090 to 0.0229 nm^{-1}. The autocorrelation function was then fit using a second-order cumulant to extract the average decay rate, Γ_1. The quantity Γ_1/q^2 was then taken as the apparent diffusion coefficient, D_{app}. D_{app} at $q = 0.0132$ nm^{-1} (60°) was used to estimate the translational diffusion coefficient, and the Stokes−Einstein relationship was used to calculate the size of an equivalent hydrodynamic sphere for this particle. This analysis provided a means to compare the relative hydrodynamic size of each micelle but was not taken as an accurate measure of the true hydrodynamic diameter. No extrapolation was performed to $q = 0$ because of the uncertainty in this process for a nonspherical particle.

In order to extract properties of a worm-like micelle from these data, D_{app} was plotted as a function of q. Given the theoretical results of Winkler et al. (*39*), D_{app} will be independent of q for $q < 1/r_g$. As q increases, two regimes may appear: an intermediate scattering vector regime ($1/r_g < q < p$) in which D_{app} increases linearly with q and a large scattering vector regime ($q > p$) in which internal bending modes become important causing D_{app} to increase as $q^{2/3}$. Here, $1/2p$ is the persistence length of the micelle. Thus, the scaling behavior of D_{app} can provide an estimate of the radius of gyration and persistence length.

Atomic Force Microscopy (AFM). AFM analysis was performed using an MFP-3D AFM from Asylum research. The images were recorded in tapping mode using moderate force ratio under ambient conditions equipped with commercial silicon tips (Olympus AC240TS) with resonance frequency $f = 70$ kHz and spring constant of $k = 2$ $^{N}/_{m}$. A typical scan range of 5 μm with a resolution of 512 × 512 pixels was used for each image. Each sample was analyzed in multiple regions. Raw data were leveled by a first and second order of plane fit correction in order to remove the sample tilt.

RESULTS

A series of peptide amphiphiles was synthesized differing only in the linkage between the palmitic tail and the N-terminus of $p53_{14-29}$ peptide in order to investigate the effect of linker length, rigidity, and hydrogen bonding potential on peptide folding and self-assembly (Scheme 1). Linkers and palmitic tail were coupled directly on the resin-bound peptide, providing a simple and efficient methodology of preparing the hybrid molecules (*40*). The A_4 linker was selected since alanines are commonly used to promote the creation of PA fibers through β-sheet formation of peptide headgroups (*3, 11*). Prolines on the other hand have been shown to disrupt H-bonding close to the micelle core and promote assembly into spherical geometries (*41*). Oligo-ethylene oxides of varying lengths were used as flexible spacers between the peptide and the hydrophobic core to investigate the effect of headgroup size without introducing additional chemical interactions between monomers. The chemical structure, along with the measured molecular mass for each peptide amphiphile, is given in the Supporting Information section (Figure S1 and Table S1).

Critical Micellar Concentration. Our hypothesis is that peptide folding occurs as a result of crowding in the micelle corona of peptide amphiphile micelles, and thus, we first aimed at determining the cmc's of the different PA analogues. The cmc's were calculated using the pyrene solubilization method (*42*): the onset of an increase in intensity ratio of the third to the first highest energy emission peaks (I_3/I_1) of pyrene emission spectrum denotes its partitioning into a more hydrophobic microenvironment. For C_{16}p53, this shift corresponds to a cmc of 2.2 μM or 4.7 μg/mL (Figure 1). We estimated the pyrene partition equilibrium constant K_v using eq 3, assuming the density of the micellar core to be that of hexadecane (0.775 g/mL) (*43*). The estimated value of 2.5×10^5 may be compared to a value of 2.0×10^5 extracted from the data of Almgren et al. for sodium hexadecanesulfonate (*43*), suggesting that the hydrophobicity of the core in the two systems is similar and is that of phase-segregated alkane chains.

The cmc values for the other PAs were calculated in the same manner and are given in Table 1. The A_4 linker had no appreciable effect on cmc, whereas an increase was recorded with increasing length of ethylene oxide linker, because of the hydrophilic nature of ethylene oxide oligomers. The unmodified peptide did not cause any appreciable change in pyrene fluorescence emission up to the highest concentration studied (5 mg/mL).

Tryptophan Fluorescence Studies. Tryptophan fluorescence spectroscopy was used to gain insight in peptide folding through steady state, quenching, and anisotropy measurements. Steady-state fluorescence of Trp is sensitive to the polarity of the microenvironment, which is expected to change upon folding

Table 1. Critical Micellar Concentration, Trp_{23} Fluorescence Emission Maximum (λ_{max}), and Trp Anisotropy Values for Unmodified $p53_{14-29}$ and $p53_{14-29}$ Peptide Amphiphiles

	cmc (μM)	λ_{max} (nm)	system anisotropy, r
p53	-	355	0.030 ± 0.004
C_{16}p53	2.2	347	0.056 ± 0.003
$C_{16}EO_4$p53	5.7	347	0.050 ± 0.004
$C_{16}EO_{12}$p53	9.6	344	0.047 ± 0.003
$C_{16}EO_{36}$p53	17.1	344	0.044 ± 0.004
$C_{16}P_3$p53	n.d.*	353	0.060 ± 0.003
$C_{16}A_4$p53	1.9	355	0.065 ± 0.004

* n.d.: not determined.

into an amphipathic helix. A maximum emission wavelength (λ_{max}) at 355 nm for Trp on the unmodified peptide revealed that the fluorophore is fully hydrated (*38*) (Figure 2A). A blue shift of λ_{max} to 347 nm for C_{16}p53 above its cmc indicated a more hydrophobic environment; reduced aqueous solvation of Trp upon self-assembly could result from Trp association (e.g., via stacking (*44*)) with other hydrophobic amino acid side chains in the same or neighboring peptides. The maximum emission wavelength varied among the peptide amphiphiles studied, suggesting different polarity for the tryptophan side chain (Table 1). Compared to C_{16}p53, λ_{max} red-shifted when A_4 or P_3 linkers were incorporated and blue-shifted for the longer EO linkers (EO_{12} and EO_{36}). It is important to note here that λ_{max} for Trp on p53 peptide dissolved in tetraethylene glycol was found to be 339 nm, reflecting the lower polarity of ethylene glycol compared to water.

We used dynamic quenching of tryptophan fluorescence by iodine ions to further probe the polarity of the microenvironment surrounding the chromophores and their accessibility from the aqueous phase. Stern−Volmer plots yielded straight lines confirming dynamic quenching of Trp by I^- (Figure 2B). A decrease of K_{SV} for C_{16}p53 in comparison to the peptide reflects decreased accessibility of the quencher and a more shielded environment of Trp (*44*).

The presence of tryptophan on the self-assembled structure also affected its rotational diffusion as monitored by fluorescence anisotropy (Table 1). In the absence of resonance energy transfer, as is the case for tryptophan, anisotropy provides a measure of the fluorophore's rotational diffusion (*38*), which is related to its microenvironment and is also coupled to the size of the structure onto which it is attached (*37, 45*). The value of Trp anisotropy in $p53_{14-29}$ ($r = 0.030 \pm 0.004$) was the same as that measured for L-tryptophan ($r = 0.031 \pm 0.004$) indicating unhindered rotation of the fluorophore within its excited-state lifetime and a hydrated environment. In contrast, Trp in self-assembled C_{16}p53 exhibited markedly higher anisotropy (Table 1). This increase could arise from Trp confinement due to steric constraints in the molecular level or from its presence on larger structures that have slower rotational diffusion. In order to discern between these two alternatives, we examined peptide anisotropy in a solution of 2,2,2-trifluoroethanol (TFE) at 29 °C. TFE at this temperature has the same viscosity as the aqueous solution used to obtain the values in Table 1 (*46*) and the peptide is in α-helical conformation (see below) but not aggregated. The obtained value of 0.057 ± 0.005 in TFE indicated that anisotropy increases primarily from the reduction in rotational freedom of Trp as a result of peptide folding and the ensuing interactions with the other hydrophobic side chains. Accordingly, disassembly of C_{16}p53 micelles and concomitant loss of peptide folding in a solution of 80% acetonitrile resulted in a decrease of anisotropy to 0.021 ± 0.004. In this case, the lower anisotropy value relative to the peptide arises from the markedly lower viscosity of the solvent.

Anisotropy values for the different PA analogs were higher than that of the unmodified peptide and varied depending on the linker (Table 1). A decrease in anisotropy was observed with increasing length of ethylene oxide linker suggesting higher rotational freedom of Trp and decreased folding. A higher anisotropy of $C_{16}A_4$p53 on the other hand indicated a more constrained microenvironment for Trp in this PA compared to C_{16}p53. Considering the high λ_{max} for $C_{16}A_4$p53, the reason for the higher anisotropy seems to differ qualitatively from the other PAs; a different type of secondary structure that induces tighter peptide packing is responsible for the observed anisotropy, as will be discussed in the following section.

Circular Dichroism Studies. Peptide folding into secondary structure elements was investigated by CD spectroscopy at concentrations of PAs exceeding their cmc. The unmodified peptide exhibited a predominantly random coil conformation with minimal helical content in aqueous solutions at 25 °C as previously reported (*23*) and shown here in Figure 3A. On the contrary, the CD spectrum of C_{16}p53 in water revealed significant folding with a maximum at 195 nm, a deep minimum at 207 nm, a shoulder at 222 nm, and low ellipticity at 230 nm. The spectrum does not resemble that of a typical α-helix, which shows minima at both 207 and 222 nm distinctly, at an intensity ratio close to 1. We suspected that Trp absorption contributes to the unusual CD spectral characteristics (*47−49*). A shift in the ratio between the two minima due to stacking with other aromatic side chains (*50*) and introduction of an additional peak around 230 nm (*48*), which may be positive or negative depending on the orientation of tryptophan relative to the peptide backbone, have both been reported. Oxidation of the tryptophan to an oxindole derivative by NBS resulted in a typical helical CD spectrum exhibiting both minima at 207 and 222 nm at approximately 1:1 ratio (Figure 3C) in accordance with a previous report (*50*). We argue that the absence of the second minimum for C_{16}p53 is indeed related to Trp interference and not the absence of α-helical structure. Oxidation of unmodified peptide did not in itself induce folding as evidenced by the minimal effects on its CD spectrum (Supporting Information Figure S2). However, we cannot exclude the possibility that the polarity change resulting from NBS oxidation did not induce changes in the type of folding. Nevertheless, fitting the NBS-oxidized C_{16}p53 spectrum using a linear combination of basis spectra based on poly(L-lysine) and poly(L-glutamic acid) (*6*) yielded an α-helical content of 63% with the remaining 37% being in random coil conformation (Supporting Information Figure S3).

The similarity of C_{16}p53 spectra in water and 10 mM PBS suggests that there is no effect of ionic strength on folding up to physiological values, and therefore, electrostatic interactions are not the main driving force for folding (Figure 3A). In the presence of 50% TFE, a solvent known to enhance peptide folding (*51*), the amount of α-helicity increased for both peptide and C_{16}p53 as expected (Figure 3B).

Folding stability was studied by monitoring ellipticity of the NBS-oxidized sample at 222 nm with increasing temperature (Figure 3D). A gradual loss of peptide secondary structure was observed; however, even at the highest temperature studied (80 °C), a substantial amount of peptide was folded, indicating a high thermal stability in the aggregate state.

We next analyzed EO-containing PAs in PBS (10 mM; pH 7.4) at 25 °C (Figure 4A). Short ethylene oxide spacers ($C_{16}EO_4$p53 and $C_{16}EO_{12}$p53) resulted in a small shift of the first minimum to 205 nm, which also became deeper, a higher molar ellipticity at 222 nm, and the clear appearance of a negative peak at 230 nm when compared to C_{16}p53. The longer linker ($C_{16}EO_{36}$p53) exhibited a similar spectrum but with higher ellipticity at 205 nm. The spectra indicated a decreasing degree of folding with increasing ethylene oxide length, which becomes more obvious when the NBS-oxidized spectra are compared

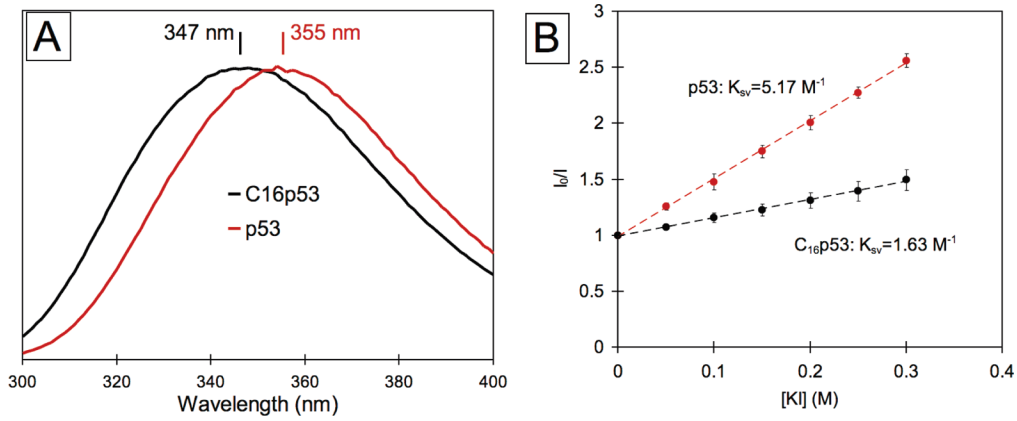

Figure 2. Comparison of Trp fluorescencence spectra of $p53_{14-29}$ and $C_{16}p53$ (A) and Stern−Volmer plots from iodine ion quenching experiments (B).

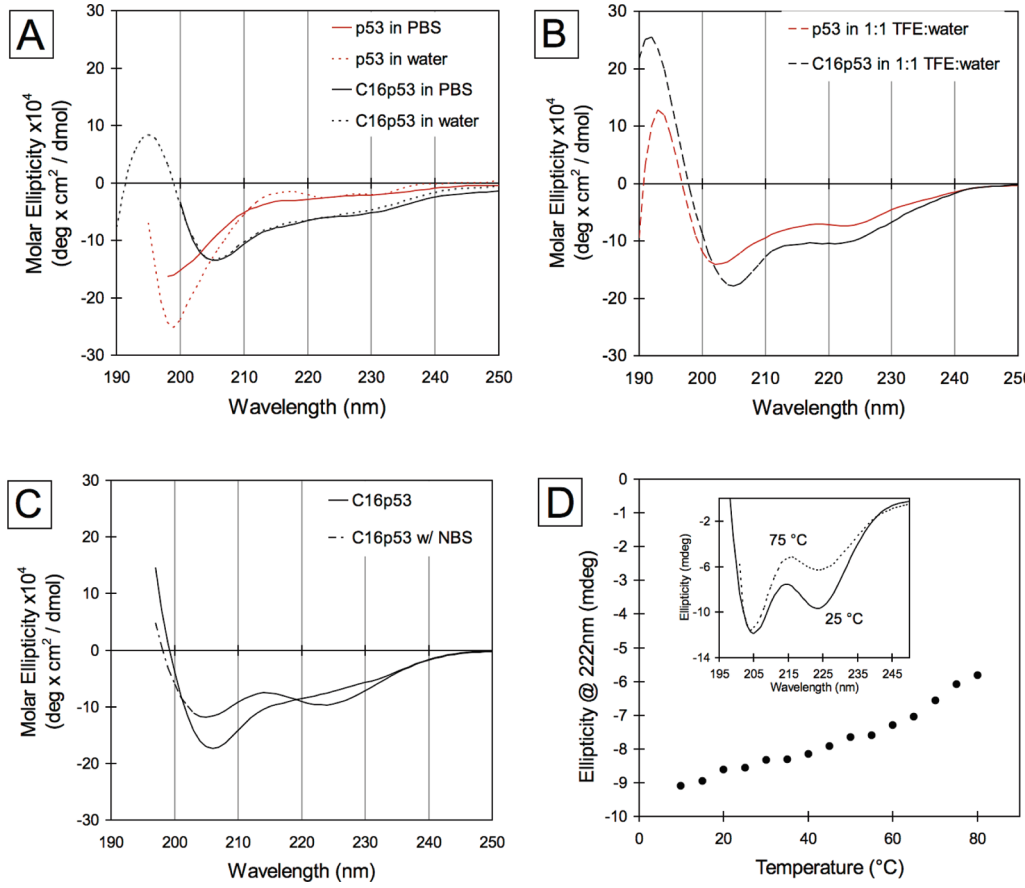

Figure 3. Circular dichroism spectra of $p53_{14-29}$ and $C_{16}p53$ in water and PBS 10 mM (A) and 2,2,2-trifluoroethanol (B). Oxidation of $C_{16}p53$ with 2 equiv. NBS resulted in a 1:1 ratio between ellipticities at 207 and 222 nm consistent with α-helix formation (C). Ellipticity at 222 nm as a function of temperature for NBS-oxidized $C_{16}p53$ (D) and corresponding spectra at 25 °C and 75°(D inset).

(Figure 5A−C). In these oxidized spectra, it is also apparent that the peak at 230 nm is due to tryptophan interference as has previously been predicted (*47*) and experimentally shown (*48, 49, 52−54*) and that the oxidized PAs clearly adopt an α-helical conformation. The peak at 230 nm is not visible in $C_{16}p53$, but this is most likely due to the lower ellipticity for this PA in the vicinity of 222 nm. We calculated α-helical contents of 54%, 45%, and 31% for oxidized $C_{16}EO_4p53$, $C_{16}EO_{12}p53$, and $C_{16}EO_{36}p53$, respectively.

In the PA with the proline linker ($C_{16}P_3p53$), changes were subtle; a slight blue shift of the negative peak at 207 nm and higher ellipticity at 222 nm suggest a slightly lower helical content compared to $C_{16}p53$ (Figure 4B). On the contrary, a dramatic change in the spectrum of $C_{16}A_4p53$ was evidenced (Figure 4B): a negative peak at 214 nm characteristic of β-sheet formation was recorded, in contrast to all previous samples. Oxidation with NBS in this case did not alter the CD spectrum (Figure 5D), which fitted to 91% β-sheet conformation.

Shape and Size of Micelles. The observed differences in peptide folding for the different PA analogues raise the question of how these affect and are in turn affected by micelle geometry. To this end, we performed multiangle dynamic light scattering measurements of PAs above their cmc's. All autocorrelation curves were satisfactorily fit using a cumulant fit to obtain a single average decay rate Γ_1 with moderate values (0.2−0.3) of the parameter Γ_2/Γ_1^2, which defines the width of the

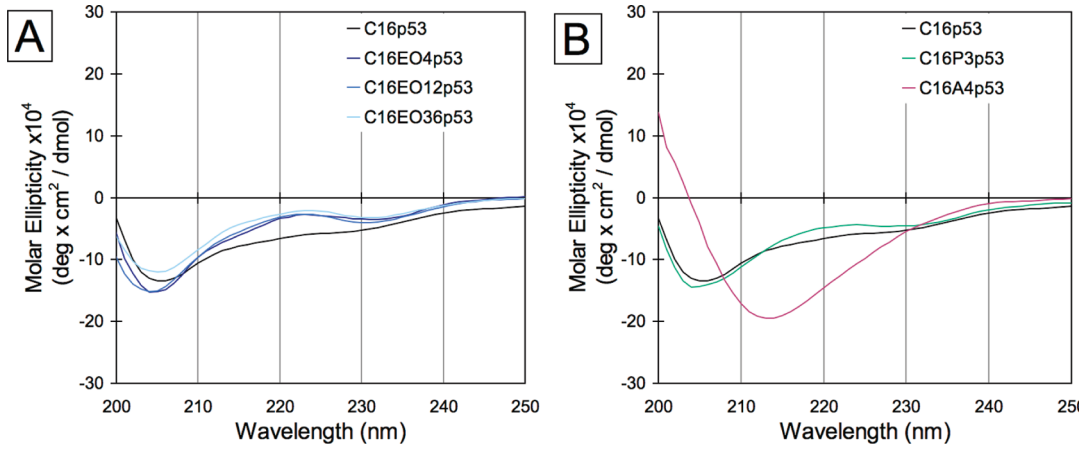

Figure 4. Circular dichroism spectra of ethylene oxide containing analogues (A) and $C_{16}A_4p53$ and $C_{16}P_3p53$ (B) in PBS 10 mM. CD spectrum of $C_{16}p53$ has been added for comparison purposes.

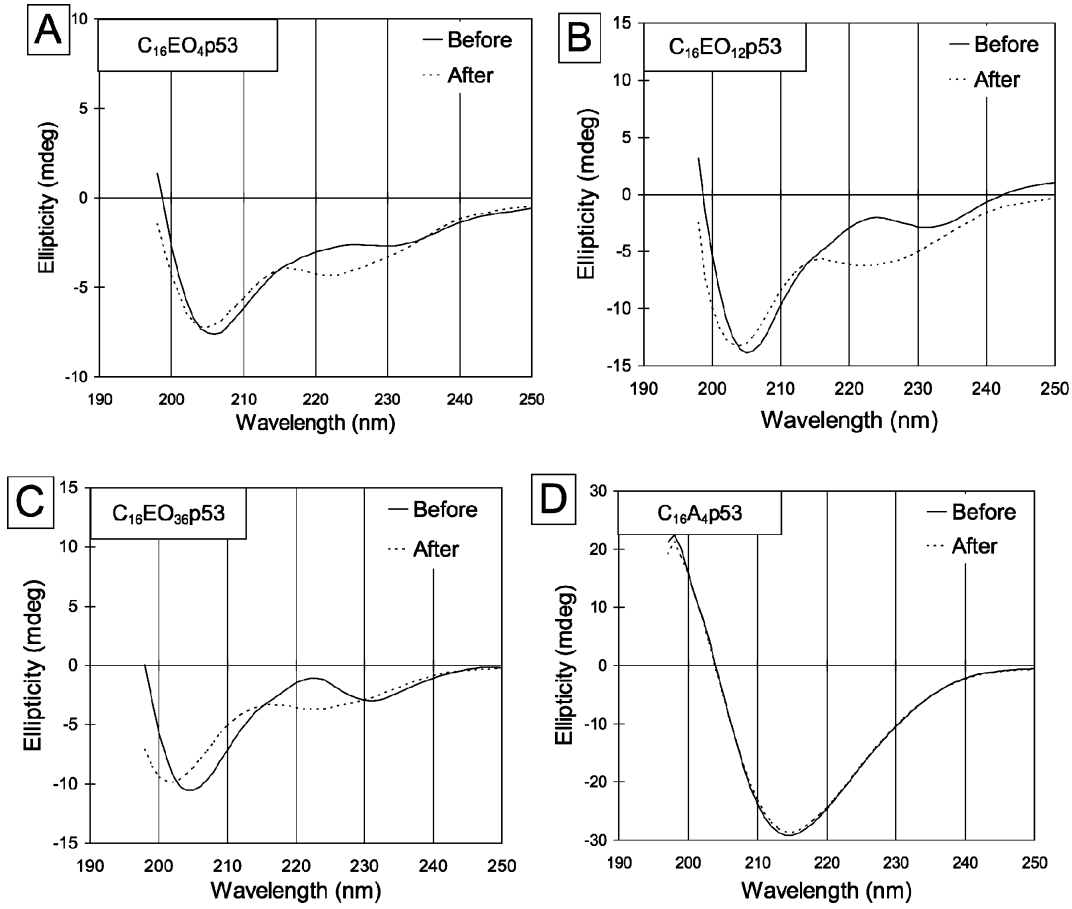

Figure 5. Comparison of CD spectra of peptide amphiphiles before and after oxidation with 2 mol equiv of *N*-bromosuccinimide (NBS). Spectra were acquired in PBS 10 mM, at 25 °C.

distribution. As an example of the pronounced *q*-dependence of the apparent diffusion coefficient $D_{app} = \Gamma_1/q^2$, results for $C_{16}p53$ aqueous solutions are presented (Figure 6). The apparent translational diffusion coefficient for the self-assembled structures was estimated at a scattering angle of 60°. Values of 1.91×10^{-8} cm^2/s and 1.73×10^{-8} cm^2/s were obtained for PBS 10 mM and water, respectively, which correspond to apparent spherical hydrodynamic diameters of 257 and 284 nm. These values exclude the formation of small spherical micelles and along with the observation of angular dependence point to formation of larger anisotropic structures. The insensitivity to ionic strength up to physiological salt concentration (0.15 M) further shows that electrostatic interactions are not the main determining factor in $C_{16}p53$ self-assembly (Figure 6). Hydrodynamic diameters of $C_{16}p53$ at a fixed angle of 90° did not seem to depend largely on concentration showing a small decrease from 0.5 to 2.5 mg/mL (Supporting Information Figure S4). Instead, an influence of temperature on size was noted: larger apparent hydrodynamic diameters were calculated when temperature increased from 5 to 55 °C (Supporting Information Figure S5).

We calculated the apparent hydrodynamic diameters for different batches of the PAs, at a scattering angle of 60° in PBS 10 mM (Figure 7). Interestingly, no major differences between analogues were noted with the exception of $C_{16}EO_{12}p53$. Even though the protocol developed for micelle formation gave far

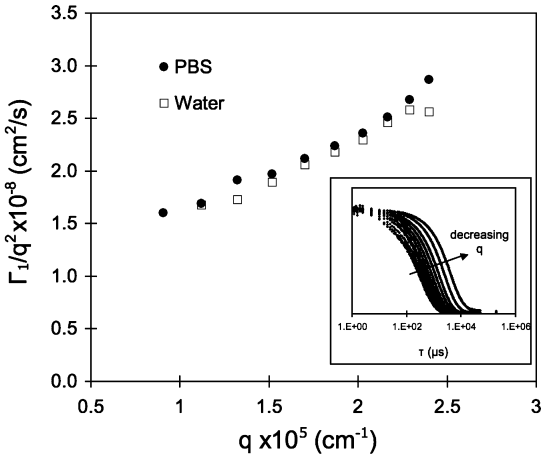

Figure 6. Angular dependence of apparent diffusion coefficient ($D_{app} = \Gamma_1/q^2$) of C_{16}p53 micelles in water and PBS 10 mM, at 25 °C. Normalized autocorrelation curves are shown in the inset for sample in PBS.

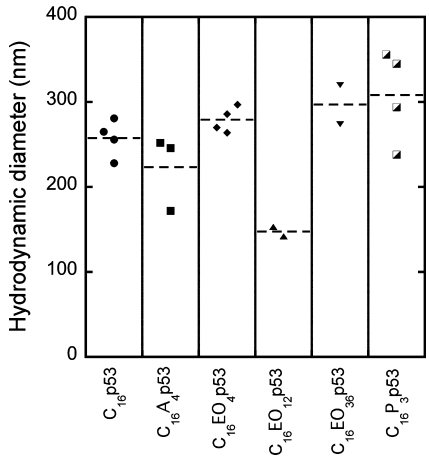

Figure 7. Hydrodynamic diameters of peptide amphiphile micelles in PBS 10 mM at 25 °C. Hydrodynamic diameters were calculated from apparent diffusion coefficients at 60° ($q = 0.0132$ nm^{-1}) and do not represent physical dimensions; they provide values for comparison between the different PA analogues. Each point represents a different batch.

more reproducible DLS results than direct dissolution of the lyophilized PAs and PAs were of high purity, we still observed some batch-to-batch variability indicating that micelle formation was sensitive to sample history and possible impurities. One of our initial hypotheses was that increasing length of the ethylene oxide linker would induce a high degree of curvature on the micelles due to larger headgroups and steric hindrances and thus a decrease in size (*7*). Although sample $C_{16}EO_{12}$p53 showed significantly faster diffusion (smaller size) than C_{16}p53, $C_{16}EO_{36}$p53 did not follow the trend.

The apparent hydrodynamic diameter provides values that are convenient for comparisons but do not correspond to actual physical dimensions. We sought shape information of the supramolecular structures by the use of atomic force microscopy. C_{16}p53 aqueous solutions deposited on freshly cleaved mica and imaged after water evaporation revealed the presence of elongated micelles (Figure 8). These images complement previously reported cryogenic transmission electron micrographs, where elongated structures were observed (*55*). We avoided extracting quantitative values for the size of the self-assembled structures based on AFM, since surface adsorption and the drying process could result in changes of the actual dimensions of the micelles in solution.

Analysis of the scaling behavior of the DLS data revealed no region in which D_{app} was independent of q (Figure 9 and

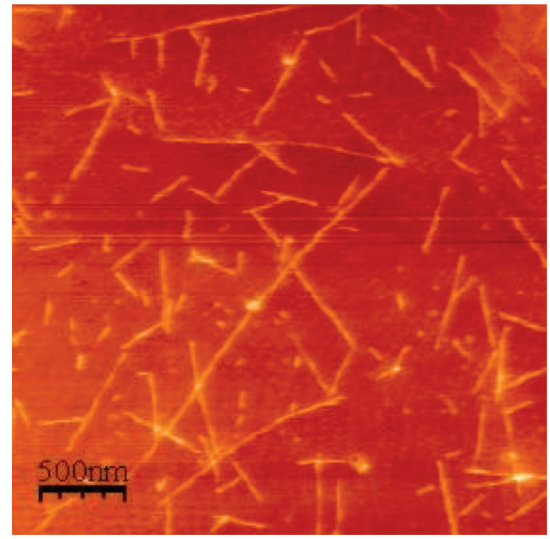

Figure 8. Atomic force micrograph showing formation of elongated micelles of C_{16}p53 deposited on mica following water evaporation.

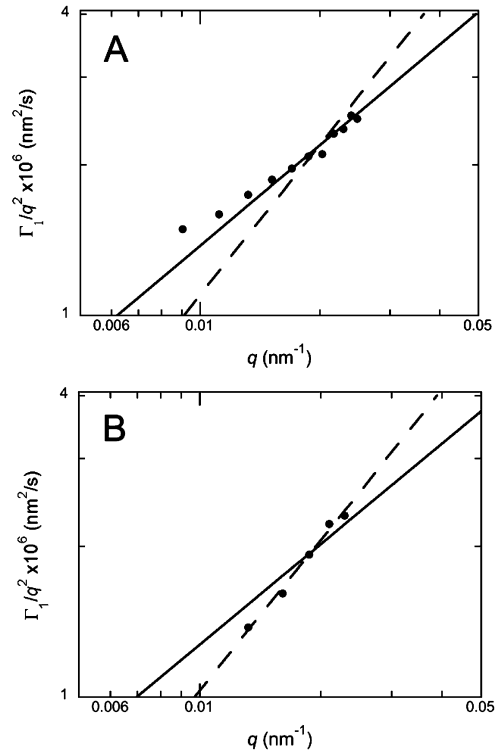

Figure 9. Angular dependence of calculated diffusion coefficient ($D_{app} = \Gamma_1/q^2$) of C_{16}p53 (A) and $C_{16}P_3$p53 (B) micelles in PBS 10 mM, at 25 °C. Solid lines correspond to the relation $D_{app}(q) \sim q^{2/3}$, while dashed lines represent $D_{app}(q) \sim q$.

Supporting Information Figure S6). Thus, the radius of gyration for all micelles is larger than ~100 nm. One exception to this statement is $C_{16}A_4$p53 micelles, for which the low scattering vector regime was found to extend to $q \approx 0.0135$ nm^{-1} corresponding to $r_g \approx 74$ nm (Supporting Information Figure S6). Scaling behavior for C_{16}p53 and $C_{16}EO_x$p53 micelles showed that $D_{app} \sim q^{2/3}$ and had no intermediate scaling region (Supporting Information Figure S6). This observation indicates that the micelles are fairly stiff, as their persistence length may approach $r_g/2$, exceeding 50 nm. In contrast, $C_{16}A_4$p53 and $C_{16}P_3$p53 micelles exhibited only the intermediate scaling region where $D_{app} \sim q$. From this, it can be concluded that $p > 0.022$ nm^{-1} and that the persistence length is less than 20 nm for these

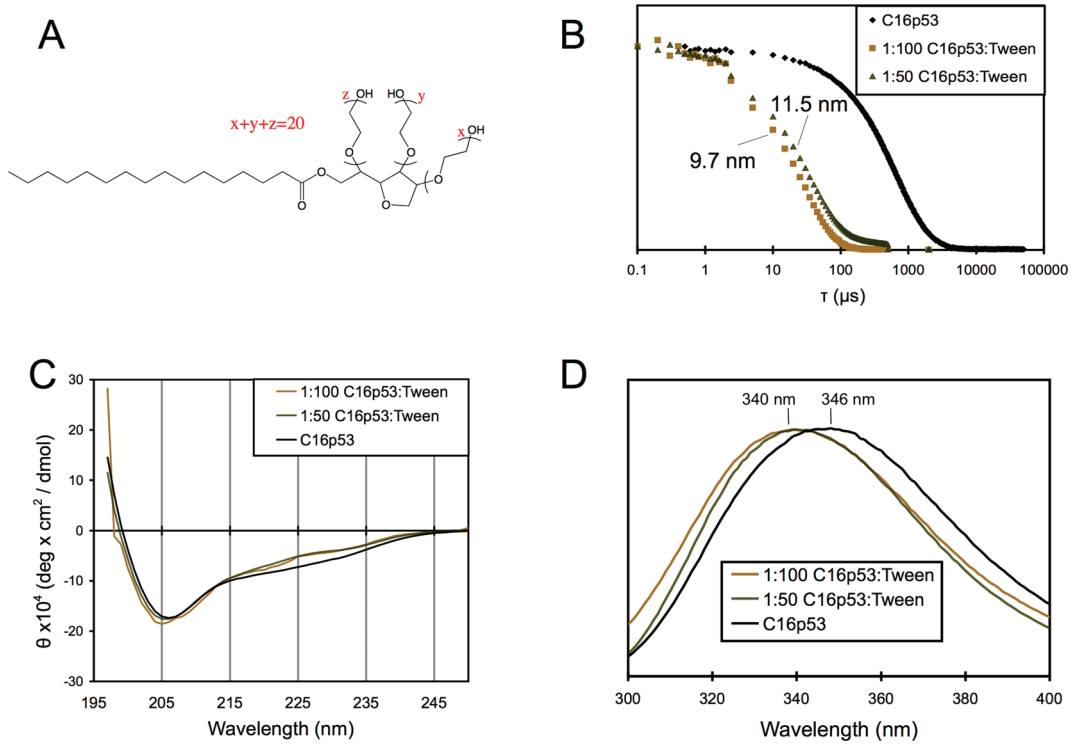

Figure 10. Mixing of C_{16}p53 with Tween 40 (A) at two different molar ratios resulted in formation of small spherical micelles. (B) Normalized autocorrelation curves of mixed micelles compared to single component C_{16}p53 micelles and calculated hydrodynamic diameters. (C) Circular dichroism spectra in PBS 10 mM at 25 °C and (D) Trp fluorescence spectra in PBS 10 mM in mixed micelles.

micelles. Thus, the A_4 and P_3 spacers result in more flexible micelles, although their overall hydrodynamic size is not significantly smaller than that of their C_{16}p53 and $C_{16}EO_x$p53 counterparts.

Formation of Small Spherical Micelles. We hypothesized that peptide folding and headgroup interactions are responsible for the elongated morphology of the self-assembled micelles instead of the highly curved micelles expected from the presence of large peptide headgroups. Indeed, in the absence of these interactions between PAs, formation of small spherical micelles occurred, consistent with monomer geometry. Mixing C_{16}p53 with Tween 40 (Figure 10A) resulted in the formation of small spherical micelles, similar in size to those formed by the surfactant alone (*56*) (Figure 10B). The two different molar ratios examined corresponded to an average of approximately one and two PAs per micelle, based on the reported aggregation number of 95 for pure Tween 40 micelles (*56*). Interestingly, circular dichroism revealed that peptides were folded, albeit to a lesser extent than single component C_{16}p53 micelles (Figure 10C). Examination of Trp fluorescence spectra showed its emission maximum at 340 nm (Figure 10D). The blue shift compared to C_{16}p53-only micelles is most likely a reflection of the ethylene glycol-rich corona formed by the Tween 40.

In contrast to C_{16}p53, the enhanced interactions between monomers of $C_{16}A_4$p53 did not allow the formation of mixed micelles. Mixing of this PA with Tween 40 at a molar ratio of 1:50 was not sufficient to disrupt H-bonding between peptide headgroups and resulted in two micelle populations as evidenced by DLS and β-sheet formation as measured by CD spectroscopy, respectively (Supporting Information Figures S6−S7).

DISCUSSION

Our present findings support conclusions from previous studies to the effect that attachment of a hydrophobic tail to an unfolded peptide and subsequent peptide amphiphile self-assembly induce secondary structure. This study further provides insight on the effect of different incorporated linkers between the palmitic tail and peptide $p53_{14-29}$ on peptide folding and supramolecular structure, demonstrating that secondary structure type and extent can be controlled by appropriate linker selection.

The main driving force for peptide amphiphile self-assembly is the hydrophobic effect of the attached hydrocarbon tails. In their absence, the unmodified peptide does not self-associate at concentrations up to 5 mg/mL, as evidenced by lack of scattering from objects larger than 2 nm or change in pyrene fluorescence spectra. The peptide remains unfolded, present mostly as a random coil, and as a consequence, tryptophan is fully hydrated and easily accessible to quenching ions. Peptide palmitoylation, micelle formation, and minimization of the interfacial area between the oily core and water results in close packing of the peptide headgroups. Loss of conformational freedom due to tethering and confinement leads to folding into defined secondary structure motifs and concomitant Trp fluorescence changes. Such behavior has been predicted using mechanistic models and lattice simulations and has been shown for a number of peptides with differing secondary structure motifs, including α-helices, triple helices, and β-sheets (*6, 14, 28, 29, 57, 58*). Peptide−peptide interactions are not necessary for folding: crowding with oligomeric ethylene oxide headgroups in Tween 40 mixed micelles also induced peptide folding.

However, our results demonstrate the importance of peptide−peptide interactions in determining the peptide secondary structure motifs of different PA analogues. These interactions were altered through the choice of linker and indicate that peptide folding is controlled by a subtle interplay of stabilizing forces. Similar conclusions were recently obtained by a study showing how secondary structure of a leucine-rich peptide was determined from the curvature of the gold particles it was attached onto (*32*). In contrast to that report, curvature in our system is not set a priori but is determined through the self-assembly process. In order to better understand our results, it is important to consider the structure of $p53_{14-29}$ in its physiological

state. There is no crystal structure available for the N-terminus of soluble p53; however, in a complex with hDM2, $p53_{18-26}$ forms an amphipathic α-helix, which inserts into a groove on the surface of hDM2 (*59*). The hydrophobic face of the helix displays the side chains of Phe_{19}, Trp_{23}, and Leu_{26}, which are critical for strong binding, with the aromatic rings of Phe and Trp stacked in close proximity to each other (*59*).

In the simplest PA where palmitic acid is directly attached to the N-terminus of the peptide via an amide bond (C_{16}p53), evidence points to a similar helical structure being formed. The unusual α-helical CD spectrum arises from Trp stacking, consistent with the blue shift that is observed in Trp fluorescence spectroscopy, a reduced accessibility to quenching iodide ions (*44*) and higher fluorescence anisotropy. The CD spectrum could be mistaken for that of a 3−10 helix (*60, 61*), but the demonstration that NBS-oxidized PAs exhibit an α-helical signature, as well as the fact that ellipticity at 195 nm is significantly higher than 0, point to an α-helical conformation. Trp_{23} seems to stack with Phe_{19}, as was found for the hDM2-bound peptide, rather than with another aromatic side chain of a neighboring peptide, since the spectra of C_{16}p53 "diluted" in Tween 40 mixed micelles were identical to those of C_{16}p53 micelles and anisotropy values of isolated peptides folded in the presence of TFE exhibited the same Trp anisotropy as that of folded C_{16}p53. We would like to note that it is not possible to exclude the scenario that NBS oxidation causes a structural change in the folded state of the peptide. Future infrared and/or NMR measurements should be pursued to clarify this point.

When hydrophilic ethylene oxide spacers of increasing length were interposed between peptide and tail, the extent of folding was lower. Again, significant changes in CD spectra upon NBS oxidation helped correlate the negative peak at 230 nm with Trp interference and quantify the decrease of folding in EO-containing analogues. A concomitant decrease in anisotropy was a result of partial unfolding, which increased rotational freedom of the fluorophor, while the blue shift in λ_{max} compared to C_{16}p53 is most likely linked to the presence of ethylene oxide in the micelle corona, which alters the local polarity of Trp. By comparison of the structures of C_{16}p53 and $C_{16}EO_x$p53, it is logical to assume that the observed changes arise from the more flexible nature of the oligo(ethylene oxide) backbone, which positions the peptide further from the core−corona interface, alleviating the molecular frustrations of the peptides, in that region. Moreover, control of α-helical content via ethylene oxide linker length could provide a powerful tool in examining its effect in situations where secondary structure is believed to be important in function.

Inclusion of four alanines linking the peptide with the palmitic tail resulted in formation of β-sheets between peptides. Consequently, Trp is no longer stacked with other side chains and its λ_{max} shows full hydration. The high anisotropy observed is presumably a consequence of the rigidity of the peptide due to the β-sheet structure along the micelle axis. The size of the A_4 linker is comparable to the shortest EO linker (EO_4); the noted difference in secondary structure is therefore a consequence of altered chemistry rather than different positioning of the peptide. Alanine is generally considered an α-helix promoter that favors a condensed state and helix formation is relatively uninhibited due to its small hydrophobic side chain (*62*); here, instead, the alanine side chain from neighboring peptides adjacent to the micelle core come in close proximity with each other, forming the condensed state with hydrogen bonds between them. This allows a tight packing and more parallel orientation of the alkane chains resulting in beneficially smaller interfacial area between the oily core and the aqueous phase. Inclusion of alanines has been shown to promote fiber formation of PAs through β-sheet formation along the fiber axis in a number of previous studies (*4, 10, 11, 13*). It appears that the stabilizing H-bonds from 4 alanines provide enough energy to overcome the tendency of the peptide to fold into an α-helix (*63*). The resulting micelles are stable such that mixing with a nonionic detergent (Tween 40) is not sufficient to disrupt the interactions between monomers, in contrast to what was observed for C_{16}p53 micelles.

Prolines are not able to form H-bonds due to their unique structure (*64*) and therefore disrupt the common secondary structure motifs α-helix and β-sheets. It has also been suggested that Pro may serve as a helix initiator when found at the N-termini of a helix, providing an initial twist and N-capping H-bonds (*65*). In our study, insertion of a rigid short proline linker did not seem to enhance helicity, but on the contrary, a decrease was noted, presumably in an analogous manner as for the EO-containing PAs.

The above findings confirm the importance of amino acid composition and H-bonding availability near the micellar core−corona interface on the folded structure of peptides in the corona. Peptide headgroup structuring and interactions are expected to additionally control the architecture of the self-assembled structure. Indeed, if we assume the peptide as a random coil and calculate the packing parameter (P) (*66*) for C_{16}p53 we obtain $p = 0.10$, predicting the formation of spherical micelles ($P \ll 1/3$): $P = (v)/(Al)$, where $l = 2.2$ nm is the length of the hydrophobic tail, $v = 0.46$ nm^3 its volume, and $A = 2.1$ nm^2 the surface area of the peptide headgroup that we can estimate from a headgroup volume of 2.32 nm^3 (using 0.73 cm^3/g as protein partial specific volume) and its 2-D projection of a peptide "sphere". The observation that elongated structures are formed is therefore consistent with peptide folding and concomitant headgroup area decrease with the peptide extending from the hydrocarbon−peptide interface. Recently, our group described the kinetic process of a simultaneous transition in secondary structure and micelle size to the above effect confirming this link (*67*). Here, no transitions were observed in the period of a week and equilibrium was reached within minutes, presumably due to differences in peptide headgroup as well as in the preparation protocol.

We did not observe major differences in the overall dimensions of the different analogues that we tested. We anticipated that increasing ethylene oxide length would promote spherical micelle formation due to steric effects of the larger headgroup. Nonionic surfactants composed of a 16-carbon tail and oligo(ethylene oxide) (also known as Brij surfactants) have been shown to transform from rod-like micelles (*68*) ($C_{16}EO_6$) to small spherical micelles having a diameter of approximately 11 nm (*69*) ($C_{16}EO_{20}$) with increasing number of ethylene oxide units. Attachment of the peptide at the end of an even longer EO linker did not have the anticipated effect on size presumably due to peptide−peptide interactions that persist even as the peptides are positioned further away from the hydrophobic core. This is consistent with the retention of a degree of peptide folding. Our understanding at this point is that the ethylene oxide segments extend away from the interface more so than would be expected if they adopted a random coil conformation. In contrast, when C_{16}p53 was mixed with an excess of Tween 40, small spherical mixed micelles were formed. This finding implies that peptide−peptide interactions are controlling micelle structure, even though they are not necessary for peptide folding as discussed previously.

Unlike overall size, we observed differences in micelle flexibility. Compared to C_{16}p53, flexibility was not affected by the addition of an EO spacer of any length but rather, by the incorporation of peptide spacers A_4 and P_3. It is possible that the P_3 spacer becomes more disruptive to packing within the micelle corona, causing correlations to decay faster along the micelle length than an extended EO layer. In the case of the A_4

spacer, we believe that β-sheet peptide structure plays a role in micelle flexibility. The coiling of β-sheet tapes may be responsible for cylindrical micelle structure and permit flexibility, as the hydrogen bonding pattern in these coiled tapes runs quasi-radially rather than axially down the micelle. Regardless of the precise mechanism, it is clear that variations in the linker between functional peptide and hydrophobic tail can affect micelle flexibility in addition to peptide secondary structure.

In conclusion, our study demonstrates that we can control the type and extent of peptide folding on self-assembled structures composed of peptide amphiphiles through inclusion of appropriate linkers in the region between the peptide of interest and the hydrophobic domain. Subtle modifications brought about strong effects, which are essential to design efficient PA assemblies. This understanding and control is required in cases where secondary structure is important for function, as in peptide−protein interactions or antibody production (*70*). In particular, the peptide we selected ($p53_{14-29}$) has been shown to exhibit enhanced binding to hDM2 when its α-helical content was increased through chemical modifications (*23*); our next steps are to examine binding of peptide amphiphile micelles to hDM2 and additionally correlate it with peptide folding.

ACKNOWLEDGMENT

This work was supported by National Heart, Lung and Blood Institute grant 5 U54 CA119335-04 and the MRSEC Program of the National Science Foundation under award DMR05-20415.

Supporting Information Available: Chemical structure (Supplementary figure S1) and molecular masses (Table S1) of peptide amphiphiles used are presented. Additional circular dichroism data (Supplementary figures S2 and S7) and dynamic light scattering results (Supplementary figures S3−S6) are also shown. This material is available free of charge via the Internet at http://pubs.acs.org.

LITERATURE CITED

(1) Jun, H. W., Paramonov, S. E., and Hartgerink, J. D. (2006) Biomimetic self-assembled nanofibers. *Soft Matter 2*, 177–181.
(2) Kokkoli, E., Mardilovich, A., Wedekind, A., Rexeisen, E. L., Garg, A., and Craig, J. A. (2006) Self-assembly and applications of biomimetic and bioactive peptide-amphiphiles. *Soft Matter 2*, 1015–1024.
(3) Beniash, E., Hartgerink, J. D., Storrie, H., Stendahl, J. C., and Stupp, S. I. (2005) Self-assembling peptide amphiphile nanofiber matrices for cell entrapment. *Acta Biomater. 1*, 387–97.
(4) Silva, G. A., Czeisler, C., Niece, K. L., Beniash, E., Harrington, D. A., Kessler, J. A., and Stupp, S. I. (2004) Selective differentiation of neural progenitor cells by high-epitope density nanofibers. *Science 303*, 1352–5.
(5) Karmali, P. P., Kotamraju, V. R., Kastantin, M., Black, M., Missirlis, D., Tirrell, M., and Ruoslahti, E. (2009) Targeting of albumin-embedded paclitaxel nanoparticles to tumors. *Nanomedicine 5*, 73–82.
(6) Bitton, R., Schmidt, J., Biesalski, M., Tu, R., Tirrell, M., and Bianco-Peled, H. (2005) Self-assembly of model DNA-binding peptide amphiphiles. *Langmuir 21*, 11888–95.
(7) Kastantin, M., Ananthanarayanan, B., Karmali, P., Ruoslahti, E., and Tirrell, M. (2009) Effect of the lipid chain melting transition on the stability of DSPE-PEG(2000) micelles. *Langmuir 25*, 7279–86.
(8) Hartgerink, J. D., Beniash, E., and Stupp, S. I. (2001) Self-assembly and mineralization of peptide-amphiphile nanofibers. *Science 294*, 1684–8.
(9) Hartgerink, J. D., Beniash, E., and Stupp, S. I. (2002) Peptide-amphiphile nanofibers: a versatile scaffold for the preparation of self-assembling materials. *Proc. Natl. Acad. Sci. U.S.A. 99*, 5133–8.
(10) Behanna, H. A., Donners, J. J., Gordon, A. C., and Stupp, S. I. (2005) Coassembly of amphiphiles with opposite peptide polarities into nanofibers. *J. Am. Chem. Soc. 127*, 1193–200.
(11) Paramonov, S. E., Jun, H. W., and Hartgerink, J. D. (2006) Self-assembly of peptide-amphiphile nanofibers: the roles of hydrogen bonding and amphiphilic packing. *J. Am. Chem. Soc. 128*, 7291–8.
(12) Cui, H., Muraoka, T., Cheetham, A. G., and Stupp, S. I. (2009) Self-assembly of giant peptide nanobelts. *Nano Lett.*
(13) Stendahl, J. C., Rao, M. S., Guler, M. O., and Stupp, S. I. (2006) Intermolecular forces in the self-assembly of peptide amphiphile nanofibers. *Adv. Funct. Mater. 16*, 499–508.
(14) Yu, Y. C., Berndt, P., Tirrell, M., and Fields, G. B. (1996) Self-assembling amphiphiles for construction of protein molecular architecture. *J. Am. Chem. Soc. 118*, 12515–12520.
(15) Murray, J. K., and Gellman, S. H. (2007) Targeting protein-protein interactions: Lessons from p53/MDM2. *Biopolymers 88*, 657–686.
(16) Landschulz, W. H., Johnson, P. F., and McKnight, S. L. (1988) The leucine zipper: a hypothetical structure common to a new class of DNA binding proteins. *Science 240*, 1759–64.
(17) Zelezetsky, I., and Tossi, A. (2006) Alpha-helical antimicrobial peptides--using a sequence template to guide structure-activity relationship studies. *Biochim. Biophys. Acta 1758*, 1436–49.
(18) Henchey, L. K., Jochim, A. L., and Arora, P. S. (2008) Contemporary strategies for the stabilization of peptides in the alpha-helical conformation. *Curr. Opin. Chem. Biol. 12*, 692–7.
(19) Ghosh, P. S., Verma, A., and Rotello, V. M. (2007) Binding and templation of nanoparticle receptors to peptide alpha-helices through surface recognition. *Chem. Commun. (Camb.)* 2796–8.
(20) Tashiro, S., Tominaga, M., Yamaguchi, Y., Kato, K., and Fujita, M. (2005) Folding a de novo designed peptide into an alpha-helix through hydrophobic binding by a bowl-shaped host. *Angew. Chem., Int. Ed. Engl. 45*, 241–4.
(21) Torres, O., Yuksel, D., Bernardina, M., Kumar, K., and Bong, D. (2008) Peptide tertiary structure nucleation by side-chain crosslinking with metal complexation and double "click" cycloaddition. *ChemBioChem 9*, 1701–5.
(22) Walensky, L. D., Kung, A. L., Escher, I., Malia, T. J., Barbuto, S., Wright, R. D., Wagner, G., Verdine, G. L., and Korsmeyer, S. J. (2004) Activation of apoptosis in vivo by a hydrocarbon-stapled BH3 helix. *Science 305*, 1466–70.
(23) Bernal, F., Tyler, A. F., Korsmeyer, S. J., Walensky, L. D., and Verdine, G. L. (2007) Reactivation of the p53 tumor suppressor pathway by a stapled p53 peptide. *J. Am. Chem. Soc. 129*, 2456–2457.
(24) Zhang, F., Sadovski, O., Xin, S. J., and Woolley, G. A. (2007) Stabilization of folded peptide and protein structures via distance matching with a long, rigid cross-linker. *J. Am. Chem. Soc. 129*, 14154–5.
(25) Kutchukian, P. S., Yang, J. S., Verdine, G. L., and Shakhnovich, E. I. (2009) All-atom model for stabilization of alpha-helical structure in peptides by hydrocarbon staples. *J. Am. Chem. Soc. 131*, 4622–4627.
(26) Chapman, R. N., Dimartino, G., and Arora, P. S. (2004) A highly stable short alpha-helix constrained by a main-chain hydrogen-bond surrogate. *J. Am. Chem. Soc. 126*, 12252–3.
(27) Ghadiri, M. R., and Choi, C. (1990) Secondary structure nucleation in peptides - transition-metal ion stabilized alpha-helices. *J. Am. Chem. Soc. 112*, 1630–1632.
(28) Forns, P., Lauer-Fields, J. L., Gao, S., and Fields, G. B. (2000) Induction of protein-like molecular architecture by monoalkyl hydrocarbon chains. *Biopolymers 54*, 531–46.
(29) Laczko, I., Hollosi, M., Vass, E., and Toth, G. K. (1998) Liposome-induced conformational changes of an epitopic peptide and its palmitoylated derivative of influenza virus hemagglutinin. *Biochem. Biophys. Res. Commun. 249*, 213–7.
(30) Wattenbarger, M. R., Chan, H. S., Evans, D. F., Bloomfield, V. A., and Dill, K. A. (1990) Surface-induced enhancement of internal structure in polymers and proteins. *J. Chem. Phys. 93*, 8343–8351.

(31) Chan, H. S., Wattenbarger, M. R., Evans, D. F., Bloomfield, V. A., and Dill, K. A. (1991) Enhanced structure in polymers at interfaces. *J. Chem. Phys. 94*, 8542–8557.
(32) Mandal, H. S., and Kraatz, H. B. (2007) Effect of the surface curvature on the secondary structure of peptides adsorbed on nanoparticles. *J. Am. Chem. Soc. 129*, 6356–7.
(33) Roberson, E. D., and Mucke, L. (2006) 100 years and counting: prospects for defeating Alzheimer's disease. *Science 314*, 781–4.
(34) Chene, P. (2003) Inhibiting the p53-MDM2 interaction: an important target for cancer therapy. *Nat. Rev. Cancer 3*, 102–9.
(35) Li, C., Liu, M., Monbo, J., Zou, G., Li, C., Yuan, W., Zella, D., Lu, W. Y., and Lu, W. (2008) Turning a scorpion toxin into an antitumor miniprotein. *J. Am. Chem. Soc. 130*, 13546–8.
(36) Berndt, P., Fields, G. B., and Tirrell, M. (1995) Synthetic lipidation of peptides and amino-acids - monolayer structure and properties. *J. Am. Chem. Soc. 117*, 9515–9522.
(37) Kastantin, M., Ananthanarayanan, B., Lin, B., Ressl, J., Black, M., and Tirrell, M. (2007) Increase of fluorescence anisotropy upon self-assembly in headgroup-labeled surfactants. *Macromol. Biosci. 7*, 189–94.
(38) Lakowicz, J. R. (1999) *Principles of fluorescence spectroscopy*, 2nd ed., Kluwer Academic/Plenum, New York.
(39) Winkler, R., Harnau, L., and Reineker, P. (1997) Distribution functions and dynamical properties of stiff macromolecules. *Macromol. Theory Simul. 6*, 1007–1035.
(40) Tu, R. S., and Tirrell, M. (2004) Bottom-up design of biomimetic assemblies. *Adv. Drug Delivery Rev. 56*, 1537–63.
(41) Guler, M. O., Claussen, R. C., and Stupp, S. I. (2005) Encapsulation of pyrene within self-assembled peptide amphiphile nanofibers. *J. Mater. Chem. 15*, 4507–4512.
(42) Astafieva, I., Zhong, X. F., and Eisenberg, A. (1993) Critical micellization phenomena in block polyelectrolyte solutions. *Macromolecules 26*, 7339–7352.
(43) Almgren, M., Grieser, F., and Thomas, J. K. (1979) Dynamic and static aspects of solubilization of neutral arenes in ionic micellar solutions. *J. Am. Chem. Soc. 101*, 279–291.
(44) Vazquez-Ibar, J. L., Guan, L., Svrakic, M., and Kaback, H. R. (2003) Exploiting luminescence spectroscopy to elucidate the interaction between sugar and a tryptophan residue in the lactose permease of Escherichia coli. *Proc. Natl. Acad. Sci. U.S.A. 100*, 12706–11.
(45) Ross, J. B., Rousslang, K. W., and Brand, L. (1981) Time-resolved fluorescence and anisotropy decay of the tryptophan in adrenocorticotropin-(1−24). *Biochemistry 20*, 4361–9.
(46) Kobayashi, K., and Nagashima, A. (1985) Measurement of the viscosity of trifluoroethanol and its aqueous-solutions under high-pressure. *Bull. JSME 28*, 1453–1458.
(47) Woody, R. W. (1994) Contributions of tryptophan side chains to the far-ultraviolet circular dichroism of proteins. *Eur. Biophys. J. 23*, 253–62.
(48) Ladokhin, A. S., Selsted, M. E., and White, S. H. (1999) CD spectra of indolicidin antimicrobial peptides suggest turns, not polyproline helix. *Biochemistry 38*, 12313–9.
(49) Mahalakshmi, R., Shanmugam, G., Polavarapu, P. L., and Balaram, P. (2005) Circular dichroism of designed peptide helices and beta-hairpins: Analysis of Trp- and Tyr-rich peptides. *ChemBioChem 6*, 2152–2158.
(50) Arnold, G. E., Day, L. A., and Dunker, A. K. (1992) Tryptophan contributions to the unusual circular dichroism of fd bacteriophage. *Biochemistry 31*, 7948–56.
(51) Roccatano, D., Colombo, G., Fioroni, M., and Mark, A. E. (2002) Mechanism by which 2,2,2-trifluoroethanol/water mixtures stabilize secondary-structure formation in peptides: a molecular dynamics study. *Proc. Natl. Acad. Sci. U.S.A. 99*, 12179–84.
(52) Friedrich, C. L., Rozek, A., Patrzykat, A., and Hancock, R. E. (2001) Structure and mechanism of action of an indolicidin peptide derivative with improved activity against gram-positive bacteria. *J. Biol. Chem. 276*, 24015–22.
(53) Vuilleumier, S., Sancho, J., Loewenthal, R., and Fersht, A. R. (1993) Circular dichroism studies of barnase and its mutants: characterization of the contribution of aromatic side chains. *Biochemistry 32*, 10303–13.
(54) Ohmae, E., Sasaki, Y., and Gekko, K. (2001) Effects of five-tryptophan mutations on structure, stability and function of Escherichia coli dihydrofolate reductase. *J. Biochem. 130*, 439–47.
(55) Missirlis, D., Khant, H., and Tirrell, M. (2009) Mechanisms of peptide amphiphile internalization by SJSA-1 cells in vitro. *Biochemistry 48*, 3304–14.
(56) Bester-Rogac, M. (2007) Micellar properties of nonionic surfactant Tween 40 (R) in water: Small-angle X-ray scattering study. *Acta Chim. Slov. 54*, 452–459.
(57) Boato, F., Thomas, R. M., Ghasparian, A., Freund-Renard, A., Moehle, K., and Robinson, J. A. (2007) Synthetic virus-like particles from self-assembling coiled-coil lipopeptides and their use in antigen display to the immune system. *Angew. Chem., Int. Ed. Engl. 46*, 9015–8.
(58) Meijer, J. T., Roeters, M., Viola, V., Lowik, D. W. P. M., Vriend, G., and van Hest, J. C. M. (2007) Stabilization of peptide fibrils by hydrophobic interaction. *Langmuir 23*, 2058–2063.
(59) Kussie, P. H., Gorina, S., Marechal, V., Elenbaas, B., Moreau, J., Levine, A. J., and Pavletich, N. P. (1996) Structure of the MDM2 oncoprotein bound to the p53 tumor suppressor transactivation domain. *Science 274*, 948–53.
(60) Silva, R. A. G. D., Yasui, S. C., Kubelka, J., Formaggio, F., Crisma, M., Toniolo, C., and Keiderling, T. A. (2002) Discriminating 3(10)- from alpha helices: Vibrational and electronic CD and IR absorption study of related Aib-containing oligopeptides. *Biopolymers 65*, 229–243.
(61) Toniolo, C., Polese, A., Formaggio, F., Crisma, M., and Kamphuis, J. (1996) Circular dichroism spectrum of a peptide 3(10)-helix. *J. Am. Chem. Soc. 118*, 2744–2745.
(62) Blaber, M., Zhang, X. J., and Matthews, B. W. (1993) Structural basis of amino-acid alpha-helix propensity. *Science 260*, 1637–1640.
(63) Velichko, Y. S., Stupp, S. I., and de la Cruz, M. O. (2008) Molecular simulation study of peptide amphiphile self-assembly. *J. Phys. Chem. B 112*, 2326–2334.
(64) Li, S. C., Goto, N. K., Williams, K. A., and Deber, C. M. (1996) Alpha-helical, but not beta-sheet, propensity of proline is determined by peptide environment. *Proc. Natl. Acad. Sci. U.S.A. 93*, 6676–81.
(65) Richardson, J. S., and Richardson, D. C. (1988) Amino acid preferences for specific locations at the ends of alpha helices. *Science 240*, 1648–52.
(66) Israelachvili, J. N. (1992) *Intermolecular and surface forces*, 2nd ed., Academic Press, San Diego.
(67) Shimada, T., Lee, S., Bates, F. S., Hotta, A., and Tirrell, M. (2009) Wormlike micelle formation in peptide-lipid conjugates driven by secondary structure transformation of the headgroups (dagger). *J. Phys. Chem. B*
(68) Cummins, P. G., Staples, E., Penfold, J., and Heenan, R. K. (1989) Geometry of micelles of the poly(oxyethylene) nonionic surfactants C16e6 and C16e8 in the presence of electrolyte. *Langmuir 5*, 1195–1199.
(69) D'Errico, G., Ciccarelli, D., and Ortona, O. (2005) Effect of glycerol on micelle formation by ionic and nonionic surfactants at 25 degrees C. *J. Colloid Interface Sci. 286*, 747–54.
(70) Muhs, A., Hickman, D. T., Pihlgren, M., Chuard, N., Giriens, V., Meerschman, C., van der Auwera, I., van Leuven, F., Sugawara, M., Weingertner, M. C., Bechinger, B., Greferath, R., Kolonko, N., Nagel-Steger, L., Riesner, D., Brady, R. O., Pfeifer, A., and Nicolau, C. (2007) Liposomal vaccines with conformation-specific amyloid peptide antigens define immune response and efficacy in APP transgenic mice. *Proc. Natl. Acad. Sci. U.S.A. 104*, 9810–5.

BC900383M